

Time-Scale Coupling Between States and Parameters in Recurrent Neural Networks

Lorenzo Livi*

August 21, 2025

Abstract

We study how gating mechanisms in recurrent neural networks (RNNs) implicitly induce adaptive learning-rate behavior, even when training is carried out with a fixed, global learning rate. This effect arises from the coupling between state-space time scales—parametrized by the gates—and parameter-space dynamics during gradient descent. By deriving exact Jacobians for leaky-integrator and gated RNNs, we obtain a first-order expansion that makes explicit how constant, scalar, and multi-dimensional gates reshape gradient propagation, modulate effective step sizes, and introduce anisotropy in parameter updates. These findings reveal that gates not only control information flow, but also act as data-driven preconditioners that adapt optimization trajectories in parameter space. We further draw formal analogies with learning-rate schedules, momentum, and adaptive methods such as Adam, pointing to possible redundancies. Empirical simulations corroborate these claims: in canonical synthetic sequence tasks (adding, copy) we show that gates induce lag-dependent effective learning rates and directional concentration of gradient flow, with multi-gate models matching or exceeding the anisotropic structure produced by Adam. These results highlight that optimizer-driven and gate-driven adaptivity are complementary but not equivalent mechanisms. Overall, this work provides a unified dynamical-systems perspective on how gating couples state evolution with parameter updates, explaining why gated architectures achieve robust trainability and stability in practice.

Contents

1	Introduction	2
2	Related Works	3
3	RNNs and Time-Scales	4
3.1	From continuous to discrete time	5
3.2	Global time rescaling	5
3.3	General time warping and gating	5
4	BPTT-based training of RNNs	6
4.1	Stochastic gradient descent in neural networks	6
4.2	Vanishing and exploding gradients	7

*OPIT – Open Institute of Technology, lorenz.livi@gmail.com

5 How time-scales in RNN states affect parameter dynamics	7
5.1 Jacobian matrices	8
5.1.1 Leaky-integrator neurons	8
5.1.2 Single scalar gate	8
5.1.3 Multiple gates	8
5.2 Time-scale interaction	9
5.2.1 Constant gate case	9
5.2.2 RNNs with scalar gate	10
5.2.3 RNNs with multiple gates	11
6 Analogies between gating mechanisms and adaptive gradient descent methods	12
7 Simulations	14
7.1 Effective learning rate induced by gates	14
7.2 Anisotropy of gradient propagation: gates vs. optimizer	16
7.3 Broader implications	18
8 Conclusions and future directions	21
A Matrix product expansion via the Fréchet derivative formulation	21
A.1 Fréchet differentiability and the first-order expansion	21
A.2 Matrix products with structured perturbations	22
A.3 Recursive application of the product rule	22
A.4 First-order expansion	23
A.5 Simulations supporting the validity of the first-order approximation	24
B Adam	29

1 Introduction

Recurrent neural networks (RNNs) remain a central tool for modeling sequential data, yet their training dynamics continue to raise theoretical and practical challenges. A large body of work has shown how gating mechanisms—as in LSTMs and GRUs—help stabilize learning by regulating information flow in hidden states and mitigating gradient pathologies. From this perspective, gates are primarily understood as filters that control memory retention and short-term state evolution.

In this work, we demonstrate that gates have an additional, previously overlooked role: they also reshape the *parameter dynamics* during optimization. Specifically, we show that gating mechanisms implicitly induce adaptive learning-rate behavior, even when training is carried out with a fixed global step size. The same time-scale modulations that gates impose on state dynamics couple into parameter updates via back-propagation, altering effective step sizes, introducing lag dependence, and concentrating gradient flow into dominant directions. Thus, gates act not only as information filters but also as data-driven preconditioners of the optimization process.

Our theoretical analysis is based on a perturbative expansion of the Jacobian products arising in back-propagation. By deriving exact Jacobians for leaky-integrator, scalar-gated, and multi-gated RNNs, we make explicit how gates renormalize effective learning rates and introduce anisotropy in parameter updates. This perspective reveals structural analogies with optimization heuristics such as learning-rate schedules, momentum, and adaptive methods like Adam—yet these behaviors emerge endogenously from gating rather than being externally imposed.

We complement this analysis with controlled simulations that probe the predicted phenomena. In Section 7.1, we quantify how gates modulate lag-dependent *effective learning rate profiles*. In Section 7.2, we introduce an *anisotropy index* to measure how gates and optimizers shape the directional structure of gradient propagation. These experiments confirm that gate-induced corrections remain bounded but systematic,

providing quantitative evidence that gates influence both the magnitude and orientation of temporal credit assignment. Section 7.3 discusses the broader implications of these findings for the trainability and stability of gated architectures.

Contributions. We propose a unified dynamical-systems framework for analyzing how gating mechanisms affect the coupled dynamics of states and parameters in RNNs. Our contributions are:

- We show analytically that gates act as parametrized time scales that modulate lag-dependent effective learning rates.
- We extend the analysis to directional effects, introducing the anisotropy index to quantify how gates and optimizers shape the dominant subspaces of gradient propagation.
- We validate these predictions through targeted simulations on canonical tasks (adding, copy), comparing leaky, scalar-gated, and multi-gated RNNs as well as adaptive optimization (Adam).

Together, these results highlight that both gating and optimizer dynamics shape not only the *magnitude* but also the *directional structure* of temporal credit assignment, with task-dependent trade-offs.

Structure. The remainder of the paper is organized as follows. Section 2 surveys the most relevant literature on gradient pathologies, linear and state-space models, constrained recurrent dynamics, and gating mechanisms. Section 3 introduces the interpretation of RNN gating mechanisms as parametrized time scales and formalizes the specific models considered in our analysis. Section 4 reviews backpropagation through time in RNNs and revisits the vanishing/exploding gradient problem in this context. Section 5 presents our main theoretical contribution: the derivation of Jacobian matrices for the considered RNN models and the link between state-space time scales and parameter-space dynamics. Section 6 discusses well-known variants of gradient descent and suggests explicit connections between their behaviour and the effects induced by gating mechanisms. Section 7 complements the theory with simulations on well-known sequence tasks. Section 8 summarizes the key insights and outlines future research directions. The paper contains an Appendix with two sections. The first one, Appendix A describes the first-order expansion technique used in this paper and provides numerical examples justifying its robustness. The second one, Appendix B provides a description of the well-known Adam algorithm.

2 Related Works

The study of recurrent neural networks (RNNs) has long been shaped by the well-known vanishing and exploding gradient problem [24], which affects the stability and learnability of long-term dependencies. While this issue traditionally focuses on the magnitude of gradients, recent work by Zucchetti and Orvieto [38] highlights a complementary phenomenon: as the memorization capacity of an RNN increases during training, the network output can become highly sensitive to small parameter variations. This heightened sensitivity arises even in the absence of vanishing or exploding gradients, suggesting that RNNs may undergo abrupt changes in behavior due to intrinsic instabilities in the learned parameter-state mapping. In a related vein, Cen et al. [3] proposed Random Orthogonal Additive Filters, a class of architectures designed to stabilize and enrich recurrent dynamics via orthogonal transformations, mitigating instability without sacrificing representational power.

Several lines of research have explored simplified linear models as a means of studying and designing recurrent dynamics with greater interpretability. Continuous-time state-space models, such as those in Gu et al. [9, 10], have enabled efficient training of sequence models with long-range dependencies by leveraging structured state-space kernels. More recently, Muca Cirone et al. [23] provided a theoretical analysis of linear state-space models (LSSMs), clarifying their expressive power and the role of parameterization in controlling stability and memory retention. These models offer a valuable bridge between classical control theory and modern deep learning approaches to sequence modeling.

From a training dynamics perspective, Lee et al. [21] analyzed wide neural networks through the lens of the neural tangent kernel, providing insights into the coupling between parameters and outputs during optimization. Although this framework is often applied to feedforward networks, it has implications for understanding the parameter–state interaction in recurrent settings, particularly in regimes where network width and gating jointly influence effective learning rates. Complementary work by Saxe et al. [30] investigated exact learning dynamics in deep linear networks, showing how singular value spectra dictate timescales of parameter evolution. This resonates with our perspective that recurrent gates modulate effective timescales in both state and parameter spaces.

Another rich research area involves constraining recurrent weight matrices to improve stability, expressivity, or trainability. Orthogonal and unitary RNNs [1, 11, 22, 35, 37] maintain constant gradient norms over time, thus alleviating the vanishing/exploding gradient problem. Lipschitz RNNs [7] extend this idea by explicitly controlling the Lipschitz constant to ensure robustness. Non-normal RNNs [16] and their variants incorporating Schur decompositions [15] have been proposed to exploit transient amplification phenomena for richer dynamics. Other designs include antisymmetric RNNs [4], which draw inspiration from Hamiltonian systems to ensure stability, coupled RNNs [28], which model interacting subsystems, and multiscale RNNs [29], which embed explicit time-scale separation into the architecture. Related architectural innovations such as the Clockwork RNN [18] also demonstrate the utility of explicitly incorporating multiple timescales into recurrent dynamics.

Gating mechanisms have received particular attention for their role in modulating information flow and improving trainability. From a theoretical standpoint, Chen et al. [5] and Gilboa et al. [8] analyzed the effects of gating on dynamical isometry and mean-field properties in RNNs, showing that gates can help preserve gradient flow and condition the optimization landscape. Related analyses in feedforward networks [25] underline the generality of dynamical isometry principles across architectures. Architecturally, stacked gated RNNs [32] and hybrid designs such as the “Just Another Network” (JANET) [33] demonstrate the versatility of gating in achieving both memory retention and efficient optimization. More recent theoretical work further strengthens this connection: Krishnamurthy et al. [20] and Can et al. [2] showed that gates can create slow modes in recurrent dynamics, directly modulating Jacobian spectra and shaping effective memory timescales. Empirical studies such as Quax et al. [26] confirmed that RNNs tend to develop adaptive timescales when trained on multi-scale sequential data, further illustrating the deep connection between gating and temporal structure.

In contrast to these prior works, which often study either stability, memory, or optimization in isolation, our work examines the *joint* dynamics of states and parameters under the influence of gating. By framing gating as a parametrized time-scale modulation and applying perturbative analysis to the Jacobian products that arise in backpropagation, we connect architectural design choices directly to their effect on parameter update anisotropy, gradient scaling, and memory retention across time scales.

3 RNNs and Time-Scales

We begin with a simple continuous-time RNN model [31]:

$$\frac{dx(t)}{dt} = \phi(W^r x(t) + W^i u(t)) - x(t), \quad x(0) = x_0, \quad (1)$$

where the state vector $x(t) \in \mathbb{R}^{N_r}$ evolves under the recurrent weights $W^r \in \mathbb{R}^{N_r \times N_r}$, input weights $W^i \in \mathbb{R}^{N_r \times N_i}$, and elementwise nonlinearity $\phi(\cdot)$.

The output is generated via a readout mapping

$$z(t) = \psi(x(t)), \quad (2)$$

which, in the common linear case, reduces to

$$z(t) = W^o x(t), \quad W^o \in \mathbb{R}^{N_o \times N_r}. \quad (3)$$

Different readout functions $\psi(\cdot)$ may be chosen depending on the task.

3.1 From continuous to discrete time

Applying a first-order Taylor expansion around t (i.e., Euler discretization) to (1) gives

$$x(t + \delta t) \approx x(t) + \delta t \frac{dx(t)}{dt}. \quad (4)$$

With unit step $\delta t = 1$, this yields the standard discrete-time RNN update

$$x_{t+1} = \phi(W^r x_t + W^i u_t), \quad (5)$$

with discrete-time output

$$z_t = \psi(x_t), \quad (6)$$

and, in the linear case,

$$z_t = W^o x_t. \quad (7)$$

3.2 Global time rescaling

Suppose we want to model a time-rescaled input $u(\alpha t)$ with (1). Let the state trajectory be reparameterized as $x(\alpha t)$ via a linear time-warping function

$$c(t) = \alpha t, \quad \alpha > 0. \quad (8)$$

Rewriting (1) with the new time variable, $T = c(t) = \alpha t$, we obtain:

$$\frac{dx(c(t))}{dt} = \frac{dx(T)}{dT} \frac{dT}{dt} = \alpha \phi(W^r x(t) + W^i u(t)) - \alpha x(t), \quad (9)$$

where we have renamed $t = T$ on the right-hand side to simplify the notation. This expression shows that a time-warping $c(t) = \alpha t$ scales both the recurrent and decay terms by the same factor α . Therefore, the original dynamics in (1) are *not* invariant under time-rescaling: the evolution is accelerated for $\alpha > 1$ and slowed down for $\alpha < 1$. In this sense, α acts as a global update rate, with $\alpha \rightarrow 0$ yielding nearly frozen dynamics and $\alpha \rightarrow \infty$ corresponding to very fast updates.

Discretizing (9) with (4) and $\delta t = 1$ yields

$$x_{t+1} = \alpha \phi(W^r x_t + W^i u_t) + (1 - \alpha) x_t, \quad (10)$$

which corresponds to *leaky integrator* neurons [14]. Here α is the *global state-update rate*, and its reciprocal $\tau = 1/\alpha \in [1, \infty)$ defines the global discrete-time scale. When $\alpha \rightarrow 0$, state updates occur very slowly, approaching a static memory.

3.3 General time warping and gating

To go beyond global rescaling and achieve invariance to more general time transformations, we allow an arbitrary *monotonic, differentiable* warping $c : \mathbb{R} \rightarrow \mathbb{R}$.

$$\frac{dx(c(t))}{dt} = \frac{dc(t)}{dt} \phi(W^r x(t) + W^i u(t)) - \frac{dc(t)}{dt} x(t), \quad (11)$$

$$= g(t) \phi(W^r x(t) + W^i u(t)) - g(t) x(t), \quad (12)$$

where

$$g(t) := \frac{dc(t)}{dt} \quad (13)$$

is the instantaneous *state-update rate*. When $g(t) \equiv \alpha$, we recover the leaky case (9).

We parametrize $g(t)$ as a *gate*:

$$g(t) = \sigma(W^{r,g}x(t) + W^{i,g}u(t)), \quad (14)$$

where $\sigma(\cdot) \in (0, 1)$ is the logistic sigmoid, $W^{r,g} \in \mathbb{R}^{1 \times N_r}$, and $W^{i,g} \in \mathbb{R}^{1 \times N_i}$ are gate parameters. This parametrization ensures that the update rate $g(t)$ remains bounded in $(0, 1)$, thereby smoothly interpolating between two extremes: $g(t) \approx 0$ corresponds to almost frozen dynamics (long time scale), while $g(t) \approx 1$ yields rapid updates (short time scale). Because $g(t)$ depends both on the current state $x(t)$ and the input $u(t)$, the effective time scale of the network becomes data- and state-dependent. This means that the model can adaptively modulate its temporal resolution on the fly, allocating fast or slow dynamics depending on the context, rather than relying on a fixed global constant α as in the leaky-integrator case.

Discretizing (12) with $\delta t = 1$ gives

$$x_{t+1} = g_t \phi(W^r x_t + W^i u_t) + (1 - g_t) x_t, \quad (15)$$

which makes the dynamics invariant to a global rescaling of time and, more generally, allows them to adapt to smoothly varying changes in the time axis through the gate g_t .

For neuron-specific time scales, we assign an individual gate $g_t^{(j)}$ to each neuron j :

$$x_{t+1} = g_t \odot \phi(W^r x_t + W^i u_t) + (1 - g_t) \odot x_t, \quad (16)$$

where \odot denotes elementwise multiplication and $g_t \in (0, 1)^{N_r}$. Here $\sigma(\cdot)$ in (14) is applied componentwise, with $W^{r,g} \in \mathbb{R}^{N_r \times N_r}$ and $W^{i,g} \in \mathbb{R}^{N_r \times N_i}$. Each neuron thus possesses its own *time-dependent update rate* (or time scale), enabling fine-grained adaptation of the network's temporal dynamics.

4 BPTT-based training of RNNs

4.1 Stochastic gradient descent in neural networks

The most basic form of the *stochastic gradient descent* (SGD) update rule for a parameter vector θ using a randomly sampled mini-batch of size $b \geq 1$ is

$$\theta_{l+1} = \theta_l - \frac{\mu}{b} \sum_{t=1}^b \frac{\partial \mathcal{E}_t}{\partial \theta_l}, \quad (17)$$

where l indexes the training iteration, $\mu > 0$ is the learning rate (or step size), and \mathcal{E}_t is the loss at sample t in the mini-batch. The stochasticity arises because each mini-batch is drawn at random from the training set, leading to noisy gradient estimates. For instance, in a regression setting one may use the squared error

$$\mathcal{E}_t = \|y_t - z_t\|^2,$$

where y_t is the target output, z_t is the model prediction, and θ collects all trainable parameters of the network.

The gradient $\frac{\partial \mathcal{E}_t}{\partial \theta_l}$ in (17) can be expanded using the chain rule. For recurrent models, the dependence of the current state x_t on all previous states $\{x_k\}_{k < t}$ must be taken into account:

$$\sum_{t=1}^b \frac{\partial \mathcal{E}_t}{\partial \theta_l} = \sum_{t=1}^b \frac{\partial \mathcal{E}_t}{\partial x_t} \sum_{k=1}^t \frac{\partial x_t}{\partial x_k} \frac{\partial x_k}{\partial \theta_l}. \quad (18)$$

Here, the term $\frac{\partial x_t}{\partial x_k}$ is the product of Jacobian factors linking the state at time t to the state at time k , which makes the computation inherently sequential.

Because the error gradients must be propagated backward through the sequence of states, this procedure is known as *backpropagation*. When applied to recurrent neural networks, where parameters are shared across time steps, the method is referred to as *backpropagation through time* (BPTT) [36].

4.2 Vanishing and exploding gradients

A central difficulty in computing (18) arises from the presence of long products of Jacobian matrices. For any $k < t$, the sensitivity of x_t with respect to x_k is given by

$$\frac{\partial x_t}{\partial x_k} = \prod_{j=k+1}^t J_j, \quad (19)$$

$$J_j = \frac{\partial x_j}{\partial x_{j-1}}, \quad (20)$$

where J_j is the Jacobian of the state update at time j .

Using the submultiplicative property of matrix norms,

$$\left\| \frac{\partial x_t}{\partial x_k} \right\| \leq \prod_{j=k+1}^t \|J_j\|, \quad (21)$$

and substituting into (18) gives the following bound on the gradient norm:

$$\left\| \frac{\partial \mathcal{E}_t}{\partial \theta_l} \right\| \leq \left\| \frac{\partial \mathcal{E}_t}{\partial x_t} \right\| \prod_{j=k+1}^t \|J_j\|. \quad (22)$$

Consider now the standard discrete-time RNN model (5). The Jacobian at step j has the form

$$J_j = D_{j-1} W^r, \quad (23)$$

where

$$D_j = \text{diag}(\phi'(a_j)) \quad (24)$$

is a diagonal matrix containing the derivatives of the activation function ϕ evaluated at the pre-activation

$$a_{j-1} = W^r x_{j-1} + W^i u_{j-1}. \quad (25)$$

In this case, (21) specializes to

$$\prod_{j=k+1}^t \|D_{j-1}\| \|W^r\|. \quad (26)$$

From (26), it is clear that if the spectral norm $\|W^r\|$ or the activation derivatives $\|D_{j-1}\|$ are consistently smaller than 1, the product will decay exponentially with $(t - k)$, leading to *vanishing gradients*. Conversely, if either factor is consistently greater than 1, the product will grow exponentially, producing *exploding gradients*. This spectral-norm dependence of the gradient magnitude is well documented in the literature [24] and motivates many of the stability constraints and reparameterizations used in modern RNN architectures.

5 How time-scales in RNN states affect parameter dynamics

In Section 5.1, we derive the exact expressions for the Jacobian matrices associated with the RNN variants introduced in Section 3. These Jacobians govern how perturbations to the hidden state propagate through time, and thus play a central role in both forward signal evolution and backward gradient flow. Building on these results, Section 5.2 analyzes how the time-scales embedded in the state-space dynamics interact with the optimization process. In particular, we show how the presence of constant, scalar, or multiple gating mechanisms influences the effective learning rate and the direction of parameter updates, thereby shaping the behaviour of the gradient descent algorithm.

5.1 Jacobian matrices

5.1.1 Leaky-integrator neurons

For the leaky-integrator model (10), the Jacobian at time j is

$$J_j = \alpha D_{j-1} W^r + (1 - \alpha) I, \quad (27)$$

where I is the identity matrix and $D_{j-1} = \text{diag}(\phi'(a_{j-1}))$ (see (24)). Relative to the standard RNN Jacobian $D_{j-1} W^r$, the constant gate α scales the recurrent contribution while adding a skip connection proportional to $(1 - \alpha)I$, thereby tempering gradient decay or explosion.

5.1.2 Single scalar gate

Consider now the scalar-gated model (15). Defining the gate pre-activation

$$a_t^g = W^{r,g} x_t + W^{i,g} u_t, \quad a_t^g \in \mathbb{R}, \quad (28)$$

the Jacobian becomes

$$J_j = \left[\phi(a_{j-1}) \frac{\partial g_{j-1}}{\partial x_{j-1}} + g_{j-1} D_{j-1} W^r \right] + \left[x_{j-1} \frac{\partial(1 - g_{j-1})}{\partial x_{j-1}} + (1 - g_{j-1}) I \right] \quad (29)$$

$$= (\phi(a_{j-1}) - x_{j-1}) J_{j-1}^g + g_{j-1} D_{j-1} W^r + (1 - g_{j-1}) I \quad (30)$$

$$= G_{j-1} + g_{j-1} D_{j-1} W^r + (1 - g_{j-1}) I, \quad (31)$$

where

$$J_j^g = \frac{\partial g_j}{\partial x_j} = \sigma'(a_j^g) W^{r,g}, \quad G_{j-1} = d_{j-1} J_{j-1}^g, \quad d_{j-1} = \phi(a_{j-1}) - x_{j-1}. \quad (32)$$

Here $J_j^g \in \mathbb{R}^{1 \times N_r}$ and G_{j-1} is rank-1, being the outer product of d_{j-1} and J_{j-1}^g . Thus, the scalar gate introduces a low-rank correction G_{j-1} in addition to rescaling the recurrent and skip terms.

5.1.3 Multiple gates

For the multi-gated model (16), the gate pre-activation is a vector $a_j^g \in \mathbb{R}^{N_r}$, yielding the Jacobian

$$J_j^g = \frac{\partial g_j}{\partial x_j} = \text{diag}(\sigma'(a_j^g)) W^{r,g} = D_j^g W^{r,g}, \quad (33)$$

with $D_j^g = \text{diag}(\sigma'(a_j^g))$. In this case, $g_j \in \mathbb{R}^{N_r}$ is a vector of unit-wise update rates.

Introducing the shorthand $\hat{d} = \text{diag}(d)$ for a diagonal matrix with vector d on the diagonal, and $\hat{g} = I - \hat{g}$, the Jacobian reads

$$J_j = \hat{\phi}(a_{j-1}) J_{j-1}^g + \hat{g}_{j-1} D_{j-1} W^r - \hat{x}_{j-1} J_{j-1}^g + \hat{\hat{g}}_{j-1} I \quad (34)$$

$$= \hat{d}_{j-1} J_{j-1}^g + \hat{g}_{j-1} D_{j-1} W^r + \hat{\hat{g}}_{j-1} I \quad (35)$$

$$= G_{j-1} + \hat{g}_{j-1} D_{j-1} W^r + \hat{\hat{g}}_{j-1} I. \quad (36)$$

Unlike the scalar case, here G_{j-1} is not rank-deficient, since it results from multiplying a diagonal matrix by a full matrix.

5.2 Time-scale interaction

In this section, we show that the interaction between state-space time scales and parameter updates gives rise to an *effective learning rate* μ^* , which generally differs from the nominal learning rate μ in (17). The precise form of μ^* depends on the chosen state-space model. To this end, without loss of generality we consider only one time-step t and expand the gradient formula in (18) as follows:

$$\frac{\partial \mathcal{E}_t}{\partial \theta_l} = \frac{\partial \mathcal{E}_t}{\partial x_t} \sum_{k=1}^t \left[\prod_{j=k+1}^t J_j \right] \frac{\partial x_k}{\partial \theta_l}. \quad (37)$$

5.2.1 Constant gate case

In the constant gate case $g_t \equiv \alpha \in (0, 1]$, the Jacobian (27) is

$$J_j = I + \alpha A_{j-1}, \quad A_{j-1} := D_{j-1} W_r - I. \quad (38)$$

The BPTT gradient can then be written as

$$\frac{\partial E_t}{\partial \theta_l} = \frac{\partial E_t}{\partial x_t} \sum_{k=1}^t \left[\prod_{j=k+1}^t (I + \alpha A_{j-1}) \right] \frac{\partial x_k}{\partial \theta_l}, \quad (39)$$

where θ_l denotes any parameter of the network (weights, biases, gating parameters, etc.).

Factoring α out of each Jacobian in the product gives

$$\prod_{j=k+1}^t (I + \alpha A_{j-1}) = \left(\prod_{j=k+1}^t \alpha \right) \prod_{j=k+1}^t (\alpha^{-1} I + A_{j-1}) = \alpha^{t-k} \mathcal{P}_{t,k}, \quad (40)$$

where we defined the normalized product

$$\mathcal{P}_{t,k} := \prod_{j=k+1}^t (\alpha^{-1} I + A_{j-1}). \quad (41)$$

Substituting back, the gradient becomes

$$\frac{\partial E_t}{\partial \theta_l} = \frac{\partial E_t}{\partial x_t} \sum_{k=1}^t \alpha^{t-k} \mathcal{P}_{t,k} \frac{\partial x_k}{\partial \theta_l}. \quad (42)$$

The factor α^{t-k} is the exact multiplicative decay applied to gradient components that travel through $(t-k)$ recurrent steps. This is equivalent to saying that during BPTT there is no “global” learning rate μ , but an “effective” learning rate that is valid in the time lag $t-k$. The effective learning rate reads:

$$\mu_{t,k}^* = \mu \alpha^{t-k} + (\text{perturbative correction terms}). \quad (43)$$

Here the perturbative correction terms stem from the residual $(1 - \alpha)I$ contribution and from activation derivatives, which slightly distort the pure exponential decay. This makes explicit that the learning rate decays exponentially with temporal distance, at a rate mainly determined by α . For $\alpha < 1$, long-range dependencies are progressively downweighted, leading to a vanishing gradient phenomenon for long temporal distances.

5.2.2 RNNs with scalar gate

When considering the Jacobian in (31), the product of Jacobians inside the gradient update formula can be rewritten as:

$$\prod_{j=k+1}^t G_{j-1} + g_{j-1} D_{j-1} W^r + (1 - g_{j-1}) I = \prod_{j=k+1}^t G_{j-1} + I + g_{j-1} (D_{j-1} W^r - I). \quad (44)$$

The gradient equation becomes:

$$\frac{\partial \mathcal{E}_t}{\partial \theta_l} = \frac{\partial \mathcal{E}_t}{\partial x_t} \sum_{k=1}^t \left[\prod_{j=k+1}^t G_{j-1} + I + g_{j-1} (D_{j-1} W^r - I) \right] \frac{\partial x_k}{\partial \theta_l}. \quad (45)$$

In what follows, and in Section 5.2.3, we use the general first-order expansion from Appendix A, applied to products of Jacobian matrices with $\epsilon = 1$. Unlike the constant- α case, here the gate contributions cannot be factored out in closed form; the product involves time-varying, input-driven gates that interact with state dynamics. The first-order expansion therefore provides a systematic way to separate the dominant gate-product scaling from the perturbative correction terms.

We rewrite each factor inside the product as

$$M_{j-1} = I + g_{j-1} A_{j-1} + G_{j-1}, \quad (46)$$

where $A_{j-1} = D_{j-1} W^r - I$ and G_{j-1} is a rank-1 matrix.

Expanding the matrix product to the first order in the rank-1 corrections G_{j-1} , we obtain

$$\prod_{j=k+1}^t M_{j-1} \approx \underbrace{\prod_{j=k+1}^t (I + g_{j-1} A_{j-1})}_{\text{dominant dynamics}} + \sum_{m=k+1}^t \left(\prod_{j=m+1}^t (I + g_{j-1} A_{j-1}) \right) G_{m-1} \left(\prod_{j=k+1}^{m-1} (I + g_{j-1} A_{j-1}) \right). \quad (47)$$

The first term describes the main dynamics without the rank-1 updates, while the second term is a sum of rank-1 corrections, each inserted at a different time step m and propagated by the main dynamics. We now factor the gate scalars g_{j-1} explicitly from the first term in (47) like we did in Section 5.2.1.

$$\prod_{j=k+1}^t (I + g_{j-1} A_{j-1}) = \left(\prod_{j=k+1}^t g_{j-1} \right) \left(\prod_{j=k+1}^t (g_{j-1}^{-1} I + A_{j-1}) \right).$$

Thus, the gate values contribute as a multiplicative attenuation factor given by the product $\prod_{j=k+1}^t g_{j-1}$, while the remaining matrices describe the dynamics normalized by g_{j-1} . Similarly, the rank-1 corrections remain rank-1 but acquire products of gates from the intervals before and after the insertion of G_{m-1} .

Collecting all terms, we can write

$$\prod_{j=k+1}^t M_{j-1} \approx \left(\prod_{j=k+1}^t g_{j-1} \right) P_{t,k} + \sum_{m=k+1}^t \left(\prod_{j=m+1}^t g_{j-1} \right) R_{t,m} G_{m-1} \left(\prod_{j=k+1}^{m-1} g_{j-1} \right) S_{k,m}, \quad (48)$$

where

$$P_{t,k} = \prod_{j=k+1}^t (g_{j-1}^{-1} I + A_{j-1}),$$

and the normalized matrices $R_{t,m}$ and $S_{k,m}$ are defined as

$$R_{t,m} = \prod_{j=m+1}^t (g_{j-1}^{-1} I + A_{j-1}), \quad S_{k,m} = \prod_{j=k+1}^{m-1} (g_{j-1}^{-1} I + A_{j-1}).$$

Plugging (48) into the gradient expression, we obtain

$$\frac{\partial E_t}{\partial \theta_l} = \frac{\partial E_t}{\partial x_t} \sum_{k=1}^t \left[\left(\prod_{j=k+1}^t g_{j-1} \right) P_{t,k} + \sum_{m=k+1}^t \left(\prod_{j=m+1}^t g_{j-1} \right) R_{t,m} G_{m-1} \left(\prod_{j=k+1}^{m-1} g_{j-1} \right) S_{k,m} \right] \frac{\partial x_k}{\partial \theta_l}. \quad (49)$$

Unlike the constant gate case, here the gates g_{j-1} are *time-varying* and driven by the input and state. Therefore, the attenuation factor is not a simple power (as with α), but a *product of gate values* along the time interval $[k+1, t]$. This product leads to the following effective learning rate:

$$\mu_{t,k}^* = \mu \prod_{j=k+1}^t g_{j-1} + (\text{perturbative correction terms}). \quad (50)$$

Here the perturbative correction terms arise from the residual $(1 - g_t)x_t$ pathway and from gate-gradient contributions. These introduce rank-1 modifications to the Jacobian products, modulating gradient propagation in a way that cannot be collapsed into a single scalar factor. Thus, while the multiplicative gate product sets the dominant time-varying decay, the perturbative corrections adjust the effective learning rate in a lag- and state-dependent manner.

5.2.3 RNNs with multiple gates

When considering the Jacobian in (36) the gradient equation becomes:

$$\frac{\partial \mathcal{E}_t}{\partial \theta_l} = \frac{\partial \mathcal{E}_t}{\partial x_t} \sum_{k=1}^t \left[\prod_{j=k+1}^t G_{j-1} + (\hat{g}_{j-1} D_{j-1} W^r) + (\hat{g}_{j-1} I) \right] \frac{\partial x_k}{\partial \theta_l}. \quad (51)$$

Each factor in the product appearing in the gradient expression reads

$$M_{j-1} = \hat{g}_{j-1} I + \hat{g}_{j-1} A_{j-1} + G_{j-1}, \quad (52)$$

where $A_{j-1} = D_{j-1} W^r$, $\Gamma_{j-1} \equiv \hat{g}_{j-1} = \text{diag}(g_{j-1}^{(1)}, \dots, g_{j-1}^{(N_r)})$ is the diagonal matrix of neuron-specific gates and $G_{j-1} = \hat{d}_{j-1} J_{j-1}^g$ is a full-rank matrix in this case.

Unlike the scalar gate case, here \hat{g}_{j-1} does not commute with A_{j-1} , and G_{j-1} is no longer rank-1. Therefore, the factorization is more involved. We can rewrite in terms of perturbation as follows:

$$M_{j-1} = \Gamma_{j-1}(\tilde{A}_{j-1}) + G_{j-1}, \quad (53)$$

where

$$\tilde{A}_{j-1} = A_{j-1} + \Gamma_{j-1}^{-1}(I - \Gamma_{j-1}),$$

with $\Gamma_{j-1}^{-1}(I - \Gamma_{j-1})$ defined element-wise as $\text{diag}((1 - g_{j-1}^{(i)})/g_{j-1}^{(i)})$ for $g_{j-1}^{(i)} > 0$.

Similarly to the scalar gate case, we expand the product to first order in G_{j-1} :

$$\prod_{j=k+1}^t M_{j-1} \approx \underbrace{\prod_{j=k+1}^t (\Gamma_{j-1} \tilde{A}_{j-1})}_{\text{dominant dynamics}} + \sum_{m=k+1}^t \left(\prod_{j=m+1}^t \Gamma_{j-1} \tilde{A}_{j-1} \right) G_{m-1} \left(\prod_{j=k+1}^{m-1} \Gamma_{j-1} \tilde{A}_{j-1} \right). \quad (54)$$

The first term describes the main dynamics through diagonal gates and normalized matrices \tilde{A}_{j-1} . The second term accounts for corrections due to G_{j-1} .

We now separate the diagonal gate products explicitly:

$$\prod_{j=k+1}^t (\Gamma_{j-1} \tilde{A}_{j-1}) = \left(\prod_{j=k+1}^t \Gamma_{j-1} \right) P_{t,k}, \quad (55)$$

where

$$P_{t,k} = \prod_{j=k+1}^t \tilde{A}_{j-1},$$

and the product $\prod_{j=k+1}^t \Gamma_{j-1}$ is a diagonal matrix with entries

$$\left(\prod_{j=k+1}^t g_{j-1}^{(1)}, \dots, \prod_{j=k+1}^t g_{j-1}^{(N_r)} \right).$$

For the rank corrections, we define

$$R_{t,m} = \prod_{j=m+1}^t \tilde{A}_{j-1}, \quad S_{k,m} = \prod_{j=k+1}^{m-1} \tilde{A}_{j-1}.$$

The full expansion to the first order becomes

$$\prod_{j=k+1}^t M_{j-1} \approx \left(\prod_{j=k+1}^t \Gamma_{j-1} \right) P_{t,k} + \sum_{m=k+1}^t \left(\prod_{j=m+1}^t \Gamma_{j-1} \right) R_{t,m} G_{m-1} \left(\prod_{j=k+1}^{m-1} \Gamma_{j-1} \right) S_{k,m}. \quad (56)$$

Plugging (56) into the gradient formula, we obtain

$$\frac{\partial E_t}{\partial \theta_l} = \frac{\partial E_t}{\partial x_t} \sum_{k=1}^t \left[\left(\prod_{j=k+1}^t \Gamma_{j-1} \right) P_{t,k} + \sum_{m=k+1}^t \left(\prod_{j=m+1}^t \Gamma_{j-1} \right) R_{t,m} G_{m-1} \left(\prod_{j=k+1}^{m-1} \Gamma_{j-1} \right) S_{k,m} \right] \frac{\partial x_k}{\partial \theta_l}. \quad (57)$$

Unlike the scalar gate case, here the gate contributions $\prod_{j=k+1}^t \Gamma_{j-1}$ form a *diagonal matrix* rather than a scalar. Consequently, the attenuation of the gradient is *neuron-specific* and depends on the entire input-driven gate trajectory:

$$\mu_{t,k}^{*(i)} = \mu \prod_{j=k+1}^t g_{j-1}^{(i)} + (\text{perturbative correction terms}), \quad (58)$$

where $\mu_{t,k}^{*(i)}$ is the effective learning rate associated with neuron i .

Here the perturbative correction terms involve interactions between gates and state updates, producing full-rank contributions that cannot be simplified into a scalar or diagonal factor. Their effect is modulated by the diagonal gate products but introduces additional couplings across neurons. In the multi-gate case:

- Each neuron has its own time-varying effective learning rate determined by its specific gate trajectory.
- Gradient propagation is anisotropic: some directions are damped strongly, while others are preserved, depending on the distribution of gate trajectories across neurons.
- The correction terms act as neuron-coupling perturbations, making the effective scaling both magnitude- and direction-dependent.

6 Analogies between gating mechanisms and adaptive gradient descent methods

We now turn to well-known variations of the basic gradient descent algorithm [27]. Our goal is to draw parallels between these algorithmic modifications and the implicit effects induced by tunable time scales in

RNN state dynamics. In particular, we examine how gates – by shaping the Jacobian structure – alter the effective optimization behaviour of plain gradient descent, in ways reminiscent of learning rate schedules, momentum terms, or adaptive update rules.

The analysis in Sections 5.2.1–5.2.3 shows that the Jacobian factors in gated RNNs naturally lead to multiplicative modulation of the backpropagated gradient. From the first-order expansion, this modulation directly translates into an *effective learning rate* that depends on the gate configuration. This behavior closely parallels well-known adaptive variants of gradient descent.

Constant gate (α). In the constant-gate (leaky integrator) case, the gate value $\alpha \in (0, 1]$ is fixed throughout training and across all units. The dominant multiplicative factor in the backward product over $(t - k)$ steps is α^{t-k} , independent of the input sequence or hidden state trajectory. Unlike the time-varying or multi-gate cases, there is no data dependence: the scaling depends solely on $(t - k)$ and α , remaining fixed during training. This is analogous to a fixed preconditioning factor in gradient descent, where every parameter update is scaled by the same precomputed value.

Single time-varying gate (g_{j-1}). With a scalar gate g_{j-1} , the gradient is modulated by a global, input-driven attenuation factor that varies over time. This is conceptually similar to a learning rate schedule (e.g., exponential decay), with the key difference that the modulation emerges from the network’s own state dynamics rather than from an externally prescribed schedule.

Multiple time-varying gates ($g_{j-1}^{(i)}$). In the multi-gate case, the modulation is neuron-specific, so each neuron i has its own effective learning rate, determined by the trajectory of its gate values. This mirrors adaptive optimizers such as Adam or RMSProp, which assign each parameter a distinct, dynamically adjusted step size.

Corrections due to G_{j-1} . The additional G_{j-1} terms, which arise naturally in the first-order expansion, introduce directional modifications to the gradient. In the single-gate case, these corrections are rank-1, acting as low-dimensional perturbations akin to momentum. In the multi-gate case, G_{j-1} is full-rank, leading to anisotropic scaling reminiscent of the preconditioning performed by Adam and other second-order adaptive methods.

Gating case	Gradient modulation	Analogy with optimizers
Constant gate (α)	Fixed scaling depending on distance ($t - k$)	SGD with a constant, precomputed scaling factor
Time-varying scalar gate (g_{j-1})	Global, input-driven scaling over time	SGD with a learning rate schedule
Multiple gates ($g_{j-1}^{(i)}$)	Per-neuron (diagonal) scaling	Adam/RMSProp (per-parameter adaptation)
Corrections (G_{j-1})	Directional modulation (rank-1 or full-rank)	Momentum / adaptive preconditioning

Table 1: Conceptual similarities between gating-induced gradient modulation and adaptive gradient descent methods.

In summary, the presence of gates in RNN dynamics not only stabilizes gradient propagation across long sequences but also induces implicit, data-driven modulation of the effective learning rate. Depending on the gating configuration, this modulation can behave like a fixed preconditioner, a dynamic learning rate schedule, or a fully adaptive per-parameter step size—mirroring the design principles of modern optimization algorithms without explicitly modifying the optimizer.

7 Simulations

7.1 Effective learning rate induced by gates

We empirically verify that, even when SGD uses a fixed global step size μ , gating mechanisms induce a lag-dependent effective learning rate that depends on the state-space model (leaky, scalar gate, multi-gate). The central object we use is the lag-conditioned sensitivity

$$S_{t,k}(\theta) = \left\| \prod_{j=k+1}^t J_j(\theta) \right\|_2,$$

whose magnitude reweights how much a gradient signal at time k influences the update due to a loss at time t . At each training checkpoint ℓ we aggregate these quantities to obtain an *empirical effective learning rate profile*. For every temporal distance $h = t - k$, we define

$$\tilde{\mu}_{\text{eff}}(h; \ell) \propto \text{median}_{(t,k): t-k=h} S_{t,k}(\theta_\ell).$$

To ensure comparability across models and checkpoints, we report a normalized version anchored at unit lag:

$$\tilde{\mu}_{\text{eff}}(h; \ell) = \frac{\text{median}_{(t,k): h} S_{t,k}(\theta_\ell)}{\text{median}_{(t,k): h=1} S_{t,k}(\theta_\ell)}.$$

This construction emphasizes the relative attenuation with lag: all curves start from 1 at $h = 1$, so differences directly reflect how fast or slow the effective learning rate decays with temporal distance. The normalization removes global scale effects due to parameter growth and isolates the temporal structure of the effective learning rate.

Predictors and overlays. To interpret the empirical effective learning rates, we compare them against a simple *gate-product predictor* derived from the zeroth-order theory of Section 5.2. For each model we define

$$P_{t,k}(\theta_\ell) = \begin{cases} \alpha^{t-k}, & \text{leaky (constant } \alpha\text{),} \\ \prod_{j=k+1}^t g_{j-1}, & \text{scalar gate,} \\ \frac{1}{N_r} \sum_{i=1}^{N_r} \prod_{j=k+1}^t g_{j-1}^{(i)}, & \text{multi-gate,} \end{cases}$$

which captures the multiplicative attenuation induced purely by the gates. We then form its lag-binned median

$$\bar{P}(h; \ell) = \text{median}_{(t,k): t-k=h} P_{t,k}(\theta_\ell).$$

From this baseline predictor, we construct two reference curves to overlay on the empirical profiles:

$$\begin{aligned} \tilde{\mu}_{\text{pred}}^{(0)}(h; \ell) &= \frac{\bar{P}(h; \ell)}{\bar{P}(1; \ell)}, & & \text{(zeroth-order theory, no fitting)} \\ \tilde{\mu}_{\text{pred}}^{(\text{fit})}(h; \ell) &= \left(\frac{\bar{P}(h; \ell)}{\bar{P}(1; \ell)} \right)^{s(\ell)}, & & \text{(empirical correction).} \end{aligned}$$

The first curve $\tilde{\mu}_{\text{pred}}^{(0)}$ is the direct theoretical prediction obtained by normalizing the gate-product decay. The second curve $\tilde{\mu}_{\text{pred}}^{(\text{fit})}$ introduces a fitted exponent $s(\ell)$ that corrects for higher-order (perturbative) effects not captured by the pure gate product. The slope $s(\ell)$ is estimated at checkpoint ℓ via a robust log–log regression

$$\log S_{t,k} \approx a(\ell) + s(\ell) \log P_{t,k},$$

restricted to the central predictor range (1%–99% quantiles) to avoid extreme-tail artifacts.

Setup. We train each model (leaky, scalar, multi-gate) with plain SGD (no momentum, no adaptivity) on a simple sequence task – adding problem. At selected checkpoints, we (i) run a fixed probe batch, (ii) build the exact one-step Jacobians J_j from Section 5.1, (iii) estimate $S_{t,k}$ via a short power method iteration (5 steps) for the products $\prod_{j=k+1}^t J_j$, a standard technique to approximate the largest singular value, (iv) compute $P_{t,k}$, and (v) produce the normalized lag profiles with theory overlays. We also track the fitted slope $s(\ell)$ across training.

Results. Across all models, the empirical profiles $\tilde{\mu}_{\text{eff}}(h; \ell)$ exhibit a clear, monotone attenuation with lag and are *well tracked* by the fitted-power overlay $\tilde{\mu}_{\text{pred}}^{(\text{fit})}(h; \ell)$; the zeroth-order overlay $\tilde{\mu}_{\text{pred}}^{(0)}(h; \ell)$ captures the right trend but is often too conservative or too aggressive depending on the model. The fitted log–log slopes extracted from the summaries (*slope*, R^2) are:

- **Leaky (constant α):** $s(\ell)$ starts around 2.17 at iteration 0 and slowly decreases to ≈ 2.05 by iteration 600 (all $R^2 \in [0.95, 0.97]$). The effective profile attenuates more steeply than the pure α^h predictor, reflecting additional contraction from the perturbative contraction terms (identity leakage and activation derivatives).
- **Scalar gate:** $s(\ell)$ is ≈ 0.30 at iteration 0 and decreases toward ≈ 0.23 by iteration 800 ($R^2 \approx 0.99$ throughout). The empirical profile decays more slowly than the product of gates, indicating that the $(1 - g_t)x_t$ pathway and gate-gradient terms partially counteract multiplicative attenuation, preserving longer-range contributions.
- **Multi-gate:** $s(\ell)$ remains in a narrow band ≈ 0.45 – 0.49 from iteration 0 to 800 ($R^2 \approx 0.99$). The attenuation is sublinear relative to the gate product but stronger than in the scalar case. While the multi-gate architecture implies neuron-wise anisotropy in principle (each unit has its own gate trajectory), our scalar sensitivity measure $S_{t,k}$ only captures the dominant contraction rate. The fitted slope $s(\ell)$ should therefore be interpreted as an aggregate effect of this anisotropic gating.

Interpretation. The slope $s(\ell)$ provides a quantitative diagnostic of how gates renormalize effective learning rates:

- $s = 0$: no lag dependence, i.e. the effective learning rate remains constant and equal to the nominal μ .
- $s = 1$: exact agreement with the zeroth-order gate-product predictor, i.e. $\tilde{\mu}_{\text{eff}}(h) \propto P_{t,k}$.
- $s > 1$: effective sensitivity decays more steeply with lag than the predictor, shortening the memory horizon and yielding more conservative updates.
- $0 < s < 1$: effective sensitivity decays more slowly with lag than the predictor, extending the memory horizon and yielding more permissive updates.

The fact that $s(\ell)$ is neither 0 nor 1 in practice confirms the presence of first-order correction terms beyond the pure gate product. Importantly, $s(\ell)$ remains relatively stable across training, suggesting that this modulation is a *structural property* of the dynamics rather than a transient effect of optimization.

Task dependence of the slope. The fitted log–log slope $s(\ell)$ is not an architecture-only quantity: it depends on how the data and objective shape the Jacobians $J_j(\theta_\ell)$ through the activation regime and the statistics of the gates. Tasks that keep units in a near-linear regime and encourage persistently open gates tend to yield $0 < s < 1$ (slower-than-predictor decay of the empirical effective learning rate with lag), whereas tasks that drive saturation or stronger filtering typically yield $s > 1$ (faster-than-predictor decay). Practically, this means the naive gate-product predictor is *renormalized* by first-order effects in a task-specific manner. Conditioning the fit on gate-product or activation-slope quantiles leads to consistent shifts in s , and longer-horizon tasks generally reduce s by encouraging memory-preserving dynamics. Thus, observed deviations of s from 1 quantify meaningful, task-induced corrections beyond the zeroth-order gate product and should be interpreted as part of the learned, problem-dependent time-scale interaction.

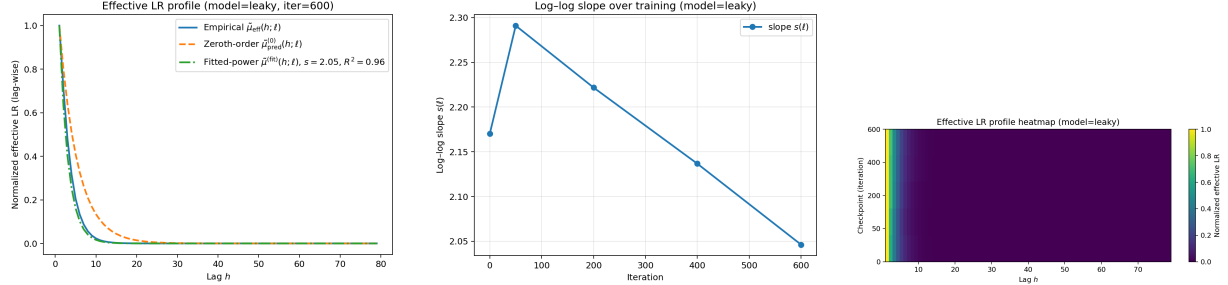


Figure 1: Leaky RNN (constant α): normalized effective LR profile at final checkpoint (left), slope $s(\ell)$ across iterations (middle), and full sensitivity heatmap $S_{t,k}$ (right).

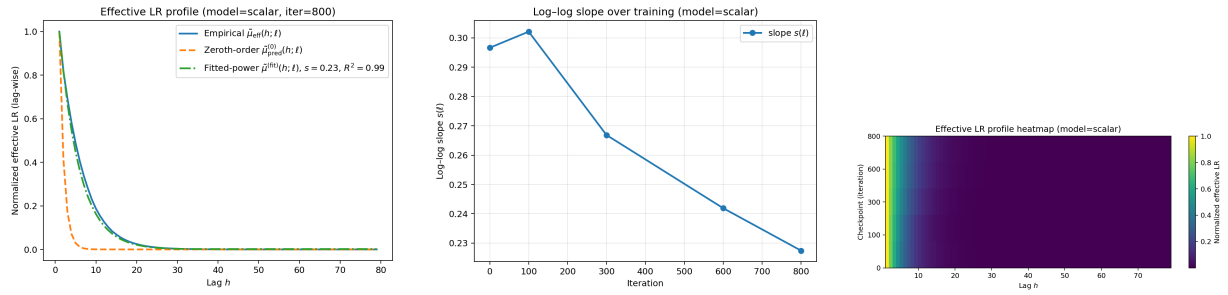


Figure 2: Scalar-gated RNN: normalized effective LR profile at final checkpoint (left), slope $s(\ell)$ across iterations (middle), and full sensitivity heatmap $S_{t,k}$ (right).

Figures. We include, for each model, (left) a representative profile at the final checkpoint with both theory overlays, (middle) the evolution of the fitted slope $s(\ell)$ across training, and (right) the sensitivity heatmap $S_{t,k}$ showing the full temporal structure.

7.2 Anisotropy of gradient propagation: gates vs. optimizer

In recurrent networks, the backpropagated error signal at time k is obtained by transporting the loss gradient at time t through the Jacobian products

$$M_{t,k} = \prod_{j=k+1}^t J_j.$$

These operators control not only the *magnitude* of gradients (how much signal survives with lag) but also their *directional structure*. Any gradient vector reaching earlier timesteps is linearly transformed by $M_{t,k}$; if the spectrum of $M_{t,k}$ is concentrated in a few large singular values, then error signals from many different losses will be funneled into the same dominant subspace. In this case, gradient flow becomes effectively low-dimensional, biasing parameter updates toward specific search directions. Conversely, if singular values remain comparable, gradients are spread across many directions, leading to more isotropic updates.

We therefore define *anisotropy of gradient propagation* as the degree of directional concentration induced by the singular spectrum

$$\sigma_1(M_{t,k}) \geq \dots \geq \sigma_{N_r}(M_{t,k}).$$

A rapid decay in σ_i with i indicates that long-range sensitivities align with a restricted set of directions, whereas a flatter spectrum reflects a more isotropic distribution of gradient energy across state space.

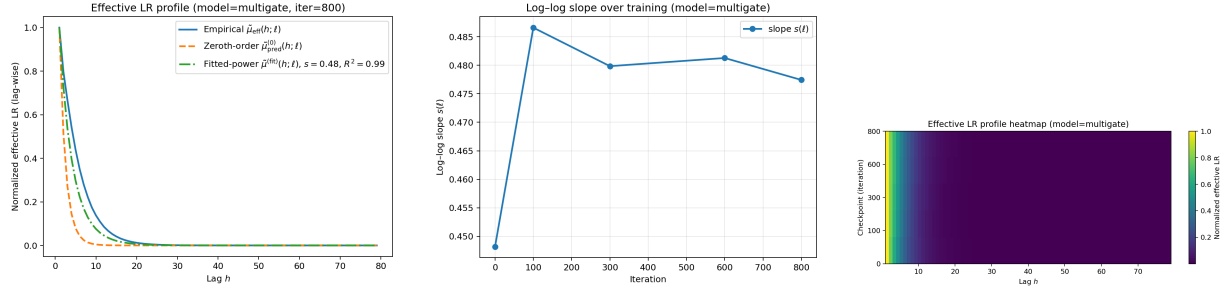


Figure 3: Multi-gated RNN: normalized effective LR profile at final checkpoint (left), slope $s(\ell)$ across iterations (middle), and full sensitivity heatmap $S_{t,k}$ (right).

This section quantifies such anisotropy and compares three models: (i) a plain RNN trained with Adam (no gates, adaptive optimizer), (ii) a scalar-gated RNN trained with SGD (15), and (iii) a multi-gated RNN (16) trained with SGD. The central question is whether neuron-wise gates with a fixed global step size induce directional concentration of temporal sensitivities that is comparable to, or stronger than, optimizer-induced preconditioning.

Quantities. For each probe sequence and checkpoint ℓ , we form Jacobian products $M_{t,k}(\theta_\ell) = \prod_{j=k+1}^t J_j(\theta_\ell)$ and compute (via svd) its singular values $\sigma_1 \geq \dots \geq \sigma_{N_r}$. We aggregate over all pairs with lag $h=(t-k)$ to obtain two lag-indexed metrics:

- *Anisotropy Index* (AI): $\text{AI}_r(h; \ell) = \text{median}_h(\sigma_1/\sigma_r)$, which is large when sensitivity mass concentrates along a leading direction. We use $r=8$.
- *Energy concentration* (CE): $\text{CE}_r(h; \ell) = \text{median}_h(\sum_{i=1}^r \sigma_i^2 / \sum_i \sigma_i^2)$, which lies in $[0, 1]$ and is high if the top r modes dominate. We use $r=8$.

Both metrics summarize the *directional geometry* of temporal credit assignment: AI emphasizes the *spread* between the first and r -th mode; CE measures how much of the total sensitivity energy sits in the top subspace.

Setup. We train the three models above on two standard sequence problems: (i) the *adding task* (real-valued, two marked positions), and (ii) a compact *copy task* (one-hot tokens followed by a delimiter, with a regression proxy target). All models have the same state dimension and are trained to comparable loss (plain RNN uses Adam, gated models use plain SGD; no momentum). At selected iterations $\ell \in \{0, 400, 800\}$ we run a fixed probe batch, build $J_j(\theta_\ell)$, form products $M_{t,k}$ for lags $h \in \{1, 2, 4, 8, 12, 16, 24, 32\}$, and record AI and CE per lag (median and interquartile range).

Results (adding task). At initialization, the multi-gated model trained with SGD already exhibits pronounced directional concentration for medium and long lags, with a larger anisotropy index ($\text{AI} = \sigma_1/\sigma_r$) than the plain RNN with Adam at several lags (Figure 4). As training proceeds, the plain RNN with Adam rapidly increases its anisotropy: by the final checkpoint (*iter 800*) it attains the *highest* AI across nearly all lags, whereas the multi-gated model remains consistently anisotropic but below Adam, and the scalar-gated model stays lowest among the three. The energy-concentration metric (CE_r) mirrors these trends: CE rises with lag for all models, with Adam ultimately achieving the strongest concentration (largest CE) at the last checkpoint, multi-gate+SGD intermediate, and scalar gate weakest. Taken together, these curves indicate that *optimizer-induced preconditioning* (Adam) can produce stronger low-dimensional amplification of temporal sensitivities than gates alone on this task; nevertheless, neuron-wise gates with a fixed step size still induce substantial, structured anisotropy without any adaptive optimizer.

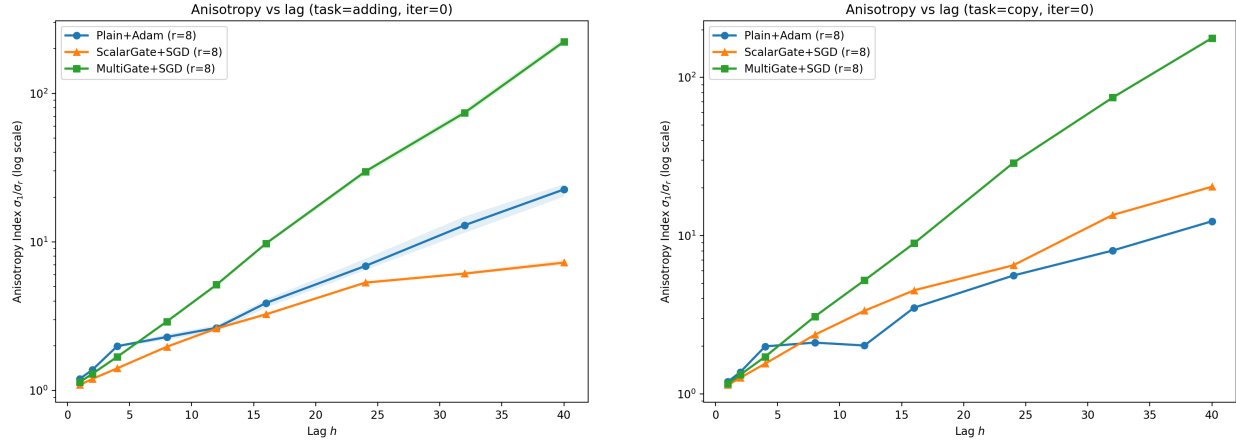


Figure 4: Early training. Anisotropy is already detectable for multi-gate and grows with lag; the relative ordering across models is preserved throughout training.

Results (copy task). On the copy task, all three models display growing anisotropy with lag and training. The multi-gated RNN with SGD consistently achieves the highest anisotropy index across checkpoints and lags, indicating that per-neuron gating is particularly effective at biasing temporal dynamics toward dominant low-dimensional directions. The plain RNN trained with Adam does increase its anisotropy compared to initialization, but remains below the multi-gate baseline throughout training. Moreover, in the CE_r plots Adam exhibits a distinct drop at larger lags (24 and 32), suggesting that the optimizer-induced concentration weakens when gradient propagation is stretched further in time. The scalar-gated model again provides only modest anisotropy, positioned between plain SGD and multi-gate but substantially below both at long horizons.

Takeaways. (i) All models exhibit increasing anisotropy with lag, confirming that long-range gradient flow becomes effectively low-dimensional. (ii) Per-neuron gates with a fixed global step size yield the most robust and consistent anisotropy, outperforming Adam across training on the copy task. (iii) Adam can boost anisotropy relative to a plain RNN, but its effect is *task-dependent*: on the adding task it eventually surpasses the multi-gate baseline, whereas on the copy task it remains weaker and loses concentration at longer lags. (iv) The scalar gate provides some concentration but markedly less than multi-gate. These findings complement the results in Section 7.1: beyond scaling the magnitude of effective learning rates with lag, gates and optimizers also sculpt *which directions* in state space carry long-range gradient information, with multi-gate architectures proving especially effective for tasks requiring persistent memory.

7.3 Broader implications

The simulations of Sections 7.1 and 7.2 reveal two complementary roles of gating and optimizer dynamics. First, gates modulate the *magnitude* of effective learning rates across lags by controlling how much past information is preserved in the state trajectory. Second, gates also shape the *directional structure* of gradient propagation, determining which subspaces of the state space remain active over long horizons.

These findings highlight that gating mechanisms do more than just stabilize training: they act as structural priors that bias the geometry of gradient flow. Optimizer adaptivity (e.g. Adam) can induce similar concentration effects, but the results show that this behavior is task-dependent: on the adding problem, Adam eventually matches or exceeds the anisotropy induced by multi-gating, while on the copy task its concentration weakens at longer lags. In contrast, per-neuron gating produces robust anisotropy across tasks. The scalar gate baseline sits between these extremes, offering partial control over anisotropy but without the

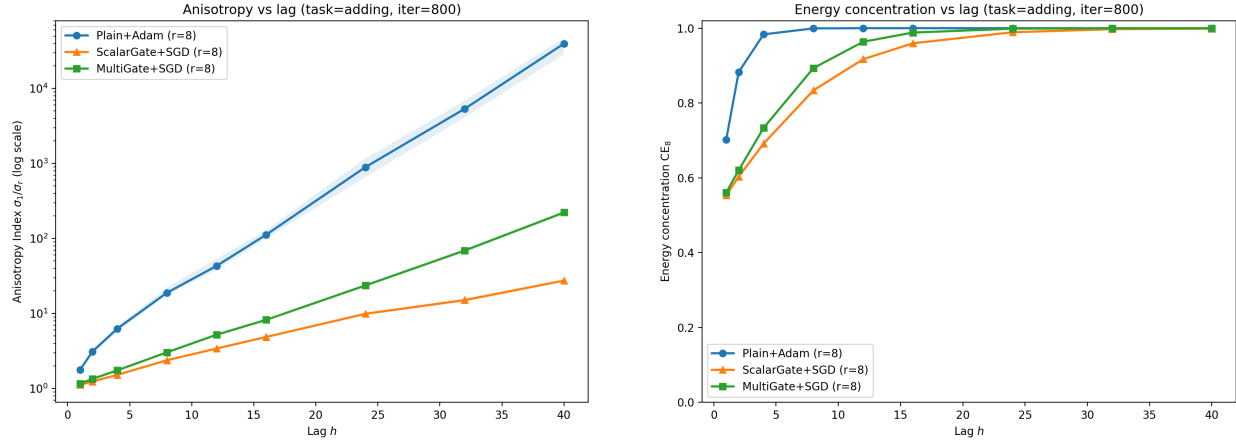


Figure 5: Adding task. Multi-gate (SGD) exhibits the strongest directionality (higher AI, higher CE) across lags; scalar gate (SGD) is intermediate; plain RNN (Adam) is lowest. Error bands show interquartile ranges across (t, k) pairs at each lag.

full flexibility of neuron-wise gating.

Taken together, these results suggest a general design principle: architectures and optimizers jointly determine not only how fast parameters move, but also *which temporal and spatial directions* dominate learning. This dual role has direct relevance for modern sequence models. In gated RNNs, the anisotropy induced by gates may interact with optimizer preconditioning in subtle ways; in attention-based models, analogous phenomena may arise through value/attention weighting. Our framework provides a lens to study such interactions systematically, pointing toward hybrid strategies where structural gating and optimizer dynamics are co-designed to control both effective learning rates and anisotropy of temporal credit assignment.

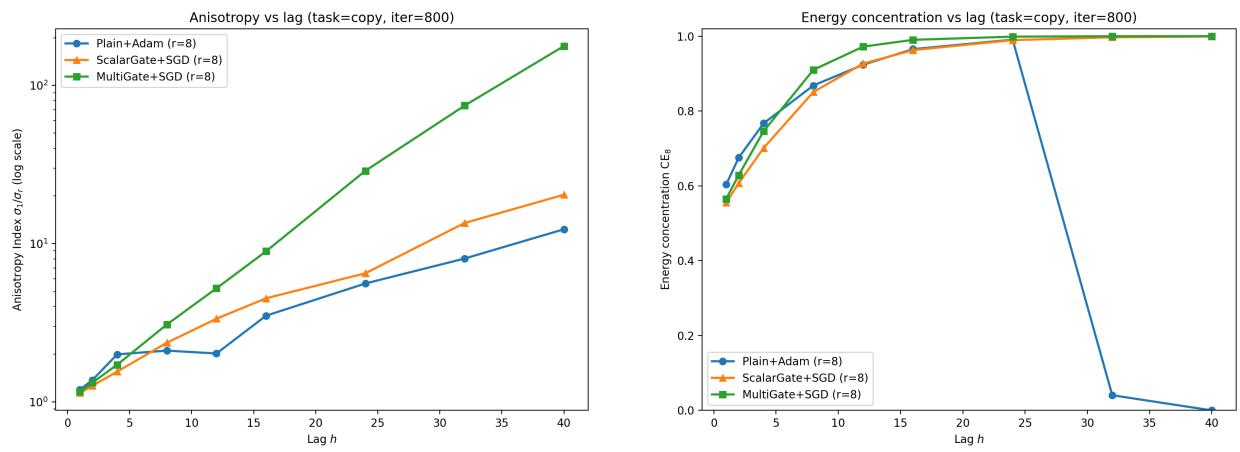


Figure 6: Copy task. Directional focusing with multi-gate is stronger and emerges at smaller lags than on the adding task; scalar gate remains intermediate; plain+Adam concentrates more gradually.

8 Conclusions and future directions

We developed a theory of time-scale interaction between state and parameter dynamics in RNNs, showing how gating mechanisms not only control information flow in state-space, but also simultaneously regulate effective learning rates and the anisotropy of gradient propagation. Our simulations confirmed that: (i) per-neuron gates reliably extend the memory horizon and induce strong anisotropy, (ii) scalar gates offer intermediate control, (iii) adaptive optimizers such as Adam can mimic or even surpass gate-induced anisotropy in some tasks, but their behavior remains task-dependent, and (iv) the interplay between gates and optimizers determines both how much and *which directions* of past information shape parameter updates.

These findings suggest that gates should be understood also as structural priors for temporal geometry, while optimizers act as dynamic reweighting mechanisms. This perspective opens new avenues for co-designing architectures and optimizers to achieve desired trade-offs in memory, stability, and efficiency of sequence learning. Extensions to LSTMs [13] and GRUs [6] and transformers [34] constitute promising directions for future work.

A Matrix product expansion via the Fréchet derivative formulation

We derive here the first-order expansion of a product of matrices with structured perturbations, starting from the *product rule for the Fréchet derivative* (Theorem 3.3 in Higham [12]).

A.1 Fréchet differentiability and the first-order expansion

Let $\mathbb{C}^{n \times n}$ denote the finite-dimensional vector space of complex $n \times n$ matrices equipped with a matrix norm (specifically, the operator 2-norm, unless otherwise stated). Since the space is finite-dimensional, all norms are equivalent.

Definition A.1 (Fréchet differentiability [12, 19]). Let $f : \mathbb{C}^{n \times n} \rightarrow \mathbb{C}^{n \times n}$. We say that f is *Fréchet differentiable* at $A \in \mathbb{C}^{n \times n}$ if there exists a bounded linear mapping

$$L_f(A, \cdot) : \mathbb{C}^{n \times n} \rightarrow \mathbb{C}^{n \times n}$$

such that

$$\lim_{\|E\| \rightarrow 0} \frac{\|f(A + E) - f(A) - L_f(A, E)\|}{\|E\|} = 0. \quad (59)$$

The operator $L_f(A, \cdot)$ is called the *Fréchet derivative* of f at A , and it is unique if it exists.

First-order expansion. If f is Fréchet differentiable at A , the first-order Taylor expansion reads

$$f(A + E) = f(A) + L_f(A, E) + o(\|E\|), \quad (60)$$

where $E \in \mathbb{C}^{n \times n}$ is the *perturbation matrix*, specifying the direction and structure of the infinitesimal change applied to A . The notation $o(\|E\|)$ means that $\|o(\|E\|)\|/\|E\| \rightarrow 0$ as $\|E\| \rightarrow 0$, i.e. the error must vanish at first order relative to the perturbation size.

Product rule. If g and h are Fréchet differentiable at A , their product $f(X) = g(X)h(X)$ satisfies the *product rule*:

$$L_{gh}(A, E) = L_g(A, E)h(A) + g(A)L_h(A, E), \quad (61)$$

where $L_g(A, E)$ denotes the Fréchet derivative of g at A in the direction E ; see [12, Sec. 3.2, Thm. 3.3] for a proof.

A.2 Matrix products with structured perturbations

We now consider a product of n factors, each with a perturbation proportional to a scalar parameter ε :

$$F(\varepsilon) = \prod_{j=1}^n (A_j + \varepsilon B_j), \quad (62)$$

where:

- $A_j \in \mathbb{C}^{d \times d}$ is the *unperturbed* factor at position j ,
- $B_j \in \mathbb{C}^{d \times d}$ is the *perturbation* at position j ,
- $\varepsilon \in \mathbb{R}$ controls the magnitude of all perturbations.

The direction of perturbation E in (60) is now the tuple

$$E \equiv (B_1, B_2, \dots, B_n),$$

meaning that in slot j the perturbation is B_j while all other slots are unchanged. Since each factor in (62) is affine in ε , $F(\varepsilon)$ is a polynomial in ε of degree at most n .

A.3 Recursive application of the product rule

For any $k \leq n, \varepsilon > 0$, define the product

$$F_k(\varepsilon) := \prod_{j=1}^k (A_j + \varepsilon B_j), \quad \text{so that} \quad F_n(\varepsilon) = F_{n-1}(\varepsilon) (A_n + \varepsilon B_n).$$

We now apply the product rule (61) to F_n by setting

$$g(\varepsilon) = F_{n-1}(\varepsilon), \quad h(\varepsilon) = A_n + \varepsilon B_n.$$

At $\varepsilon = 0$ we have:

$$g(0) = F_{n-1}(0) = A_1 A_2 \dots A_{n-1}, \quad h(0) = A_n, \quad L_h(0, E) = B_n.$$

The product rule gives:

$$L_{F_n}(0, E) = L_g(0, E) A_n + (A_1 \dots A_{n-1}) B_n. \quad (63)$$

- The first term *passes the derivative back* into the earlier factors F_{n-1} , leaving A_n unperturbed.
- The second term keeps the first $n - 1$ factors unperturbed and inserts the perturbation B_n in the last position.

By continuing this recursion for general n , we obtain the following first-order Fréchet derivative

$$L_{F_n}(0, E) = \sum_{i=1}^n \left(\prod_{j=1}^{i-1} A_j \right) B_i \left(\prod_{j=i+1}^n A_j \right), \quad (64)$$

where the empty product is taken to be the identity matrix.

Illustration for $n = 3$ Write

$$F_3(\varepsilon) = (A_1 + \varepsilon B_1)(A_2 + \varepsilon B_2)(A_3 + \varepsilon B_3), \quad F_2(\varepsilon) = (A_1 + \varepsilon B_1)(A_2 + \varepsilon B_2), \quad F_1(\varepsilon) = A_1 + \varepsilon B_1,$$

and take the perturbation direction to be the tuple $E = (B_1, B_2, B_3)$.

Step 1 (apply product rule to F_3). Set

$$g(\varepsilon) = F_2(\varepsilon), \quad h(\varepsilon) = A_3 + \varepsilon B_3.$$

Then at $\varepsilon = 0$:

$$g(0) = F_2(0) = A_1 A_2, \quad h(0) = A_3, \quad L_h(0, E) = B_3.$$

Using (61),

$$L_{F_3}(0, E) = L_g(0, E) h(0) + g(0) L_h(0, E) = L_{F_2}(0, E) A_3 + (A_1 A_2) B_3. \quad (65)$$

Step 2 (expand $L_{F_2}(0, E)$). Apply the product rule to F_2 by setting

$$g(\varepsilon) = F_1(\varepsilon), \quad h(\varepsilon) = A_2 + \varepsilon B_2.$$

Then at $\varepsilon = 0$:

$$g(0) = F_1(0) = A_1, \quad h(0) = A_2, \quad L_h(0, E) = B_2.$$

Hence

$$L_{F_2}(0, E) = L_{F_1}(0, E) A_2 + A_1 B_2. \quad (66)$$

Step 3 (expand $L_{F_1}(0, E)$). Here $F_1(\varepsilon) = A_1 + \varepsilon B_1$ is a single affine factor, so

$$L_{F_1}(0, E) = B_1. \quad (67)$$

Assemble. Substitute (66) into (65), and then use (67):

$$\begin{aligned} L_{F_3}(0, E) &= (L_{F_1}(0, E) A_2 + A_1 B_2) A_3 + (A_1 A_2) B_3 \\ &= (B_1 A_2) A_3 + (A_1 B_2) A_3 + A_1 A_2 B_3 \\ &= B_1 A_2 A_3 + A_1 B_2 A_3 + A_1 A_2 B_3. \end{aligned}$$

Thus each term contains exactly one perturbation B_i in position i , with all other slots occupied by their unperturbed counterparts A_j .

A.4 First-order expansion

Applying the first-order Taylor expansion (60) to (62) gives

$$F(\varepsilon) = F(0) + \varepsilon L_F(0, E) + O(\varepsilon^2), \quad (68)$$

where $F(0) = \prod_{j=1}^n A_j$ and $L_F(0, E)$ is given by (64). Substituting, we obtain the explicit first-order expansion:

$$F(\varepsilon) = \left(\prod_{j=1}^n A_j \right) + \varepsilon \sum_{m=1}^n \left(\prod_{j=m+1}^n A_j \right) B_m \left(\prod_{j=1}^{m-1} A_j \right) + O(\varepsilon^2). \quad (69)$$

A.5 Simulations supporting the validity of the first-order approximation

The first-order expansion (69) is accurate when all $\|B_j\|$ are small compared to $\|A_j\|$ (in operator norm), so that the accumulated $O(\varepsilon^2)$ terms remain negligible. In the main text, B_j represents gate-induced corrections, which are typically low-norm compared to the dominant dynamics in A_j . To support the validity of the expansion (69) in our setting, we perform numerical checks on the Jacobian factors extracted from the RNN models considered. Two complementary diagnostics are used: (i) for a range of ε values, we evaluate the truncation error

$$\|F(\varepsilon) - [F(0) + \varepsilon L_F(0, B)]\|$$

and verify that it scales as $O(\varepsilon^2)$, as predicted by the theory; (ii) in the operating regime of the paper ($\varepsilon = 1$), we measure the per-step operator-norm ratio $r_j = \|B_j\|_2/\|A_j\|_2$ over the time horizon. The first diagnostic confirms the expected order of accuracy of the expansion, while the second verifies that the B_j terms remain small compared to A_j in practice, ensuring that the neglected $O(\varepsilon^2)$ contributions are indeed negligible even at $\varepsilon = 1$.

Scalar gate case

Figures 7–10 report the results for the single scalar gate configuration. The truncation error in Fig. 7 follows a clear ε^2 scaling across the entire range up to $\varepsilon = 1$, indicating that the first-order expansion maintains second-order accuracy even in the actual operating regime of the network. The corresponding second-order remainder $C_2(\varepsilon) = \|F - T_1\|/\varepsilon^2$ (Fig. 8) approaches a constant for small ε and stays extremely small for ε near 1, showing that higher-order contributions are negligible in practice.

The per-step Jacobian norm comparison in Fig. 9 shows that gate corrections B_j are consistently an order of magnitude smaller than the dominant A_j terms, with the ratio distribution in Fig. 10 tightly concentrated below 0.1. This confirms that the smallness condition $\|B_j\| \ll \|A_j\|$ holds well throughout the sequence, even in the $\varepsilon = 1$ regime.

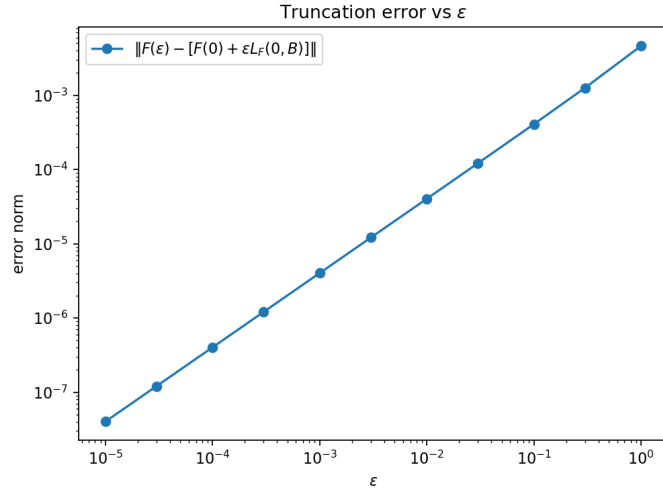


Figure 7: First-order truncation error vs. ε for the scalar gate case.

Multi-gate case

Figures 11–14 show the corresponding diagnostics for the multi-gate configuration. The truncation error in Fig. 11 also follows the predicted ε^2 scaling across the full range up to $\varepsilon = 1$, with no significant loss of accuracy in the large- ε regime relevant to our models. The second-order remainder $C_2(\varepsilon)$ in Fig. 12

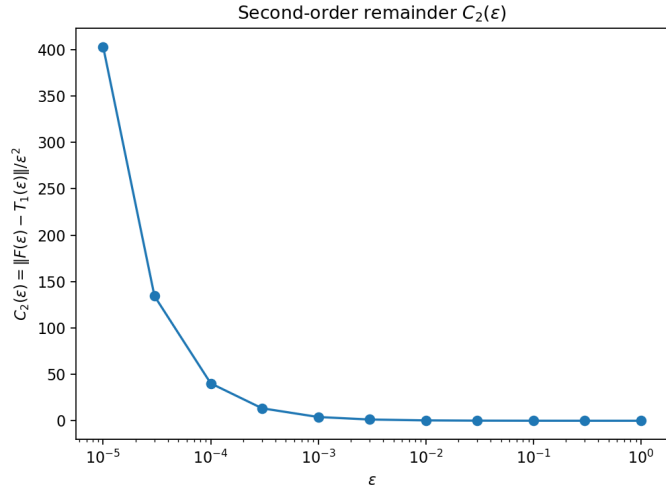


Figure 8: Second-order remainder $C_2(\varepsilon)$ for the scalar gate case.

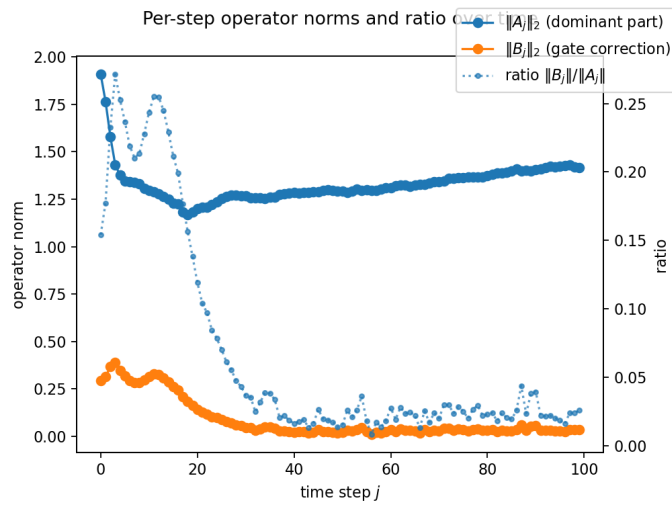


Figure 9: Per-step norms $\|A_j\|_2$ (dominant part), $\|B_j\|_2$ (gate correction), and their ratio over time for the scalar gate case.

flattens to a constant in the small- ε limit and remains very small for $\varepsilon = 1$, again indicating that neglected higher-order terms are practically irrelevant.

The per-step norm analysis in Fig. 13 confirms that gate corrections B_j are consistently small compared to A_j , with the ratio distribution in Fig. 14 concentrated well below 0.1. These results demonstrate that the smallness condition $\|B_j\| \ll \|A_j\|$ is robustly satisfied in the multi-gate case as well, validating the use of the first-order expansion in both architectures studied.

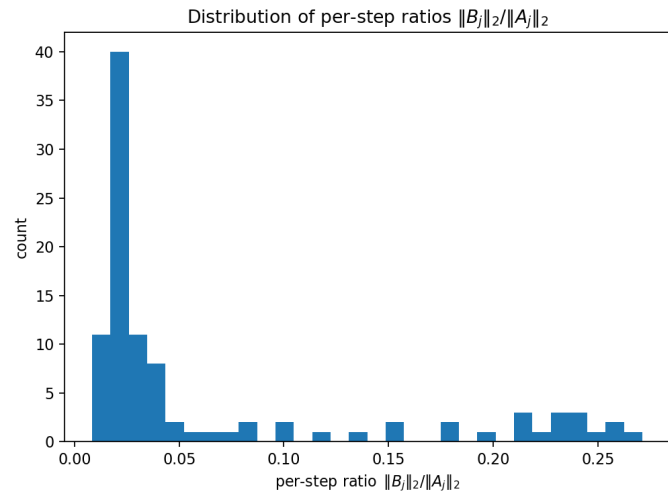


Figure 10: Distribution of per-step ratios $\|B_j\|_2/\|A_j\|_2$ for the scalar gate case.

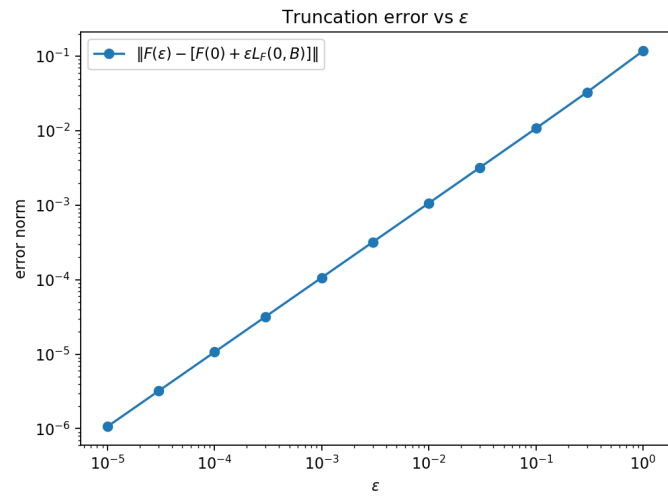


Figure 11: First-order truncation error vs. ε for the multi-gate case.

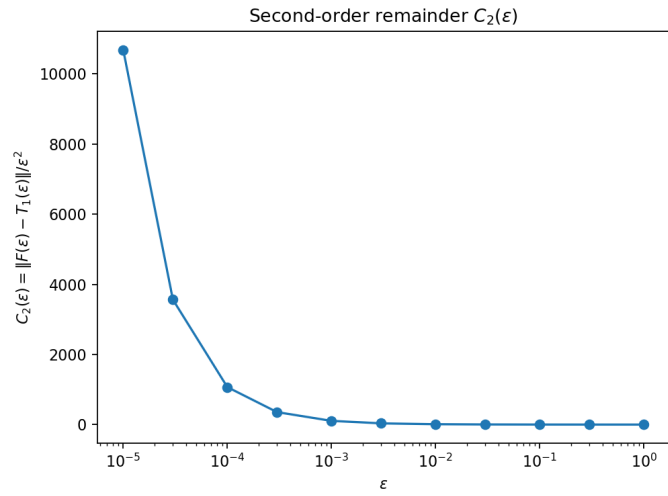


Figure 12: Second-order remainder $C_2(\varepsilon)$ for the multi-gate case.

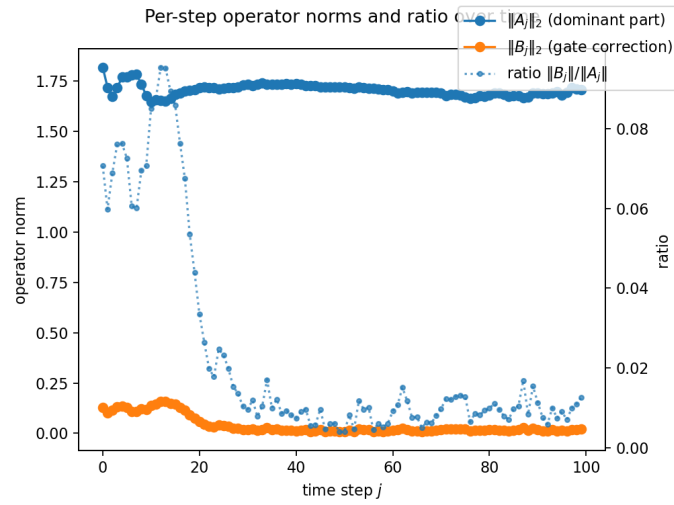


Figure 13: Per-step norms $\|A_j\|_2$ (dominant part), $\|B_j\|_2$ (gate correction), and their ratio over time for the multi-gate case.

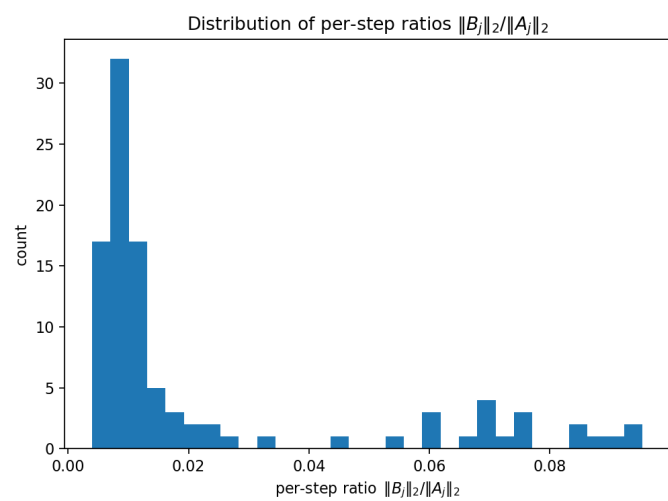


Figure 14: Distribution of per-step ratios $\|B_j\|_2/\|A_j\|_2$ for the multi-gate case.

B Adam

Adam [17] combines ideas from momentum methods and adaptive learning rate algorithms. Like Adadelta and RMSprop, it maintains an exponentially decaying average of past squared gradients $v_{t,l}$, but it also tracks an exponentially decaying average of past (unsquared) gradients $m_{t,l}$, akin to momentum:

$$m_{t,l} = \beta_1 m_{t,l-1} + (1 - \beta_1) \frac{\partial \mathcal{E}_t}{\partial \theta_l}, \quad (70)$$

$$v_{t,l} = \beta_2 v_{t,l-1} + (1 - \beta_2) \left(\frac{\partial \mathcal{E}_t}{\partial \theta_l} \right)^2, \quad (71)$$

where $\beta_1, \beta_2 \in (0, 1)$ are decay rates, and the squaring in $v_{t,l}$ is applied component-wise.

To correct the initialization bias introduced by these moving averages, Adam computes bias-corrected estimates:

$$\hat{m}_{t,l} = \frac{m_{t,l}}{1 - \beta_1^l}, \quad (72)$$

$$\hat{v}_{t,l} = \frac{v_{t,l}}{1 - \beta_2^l}. \quad (73)$$

The parameter update is then:

$$\theta_{l+1} = \theta_l - \frac{\mu}{b} \sum_{t=1}^b \frac{\hat{m}_{t,l}}{\sqrt{\hat{v}_{t,l}} + \epsilon}, \quad \epsilon > 0, \quad (74)$$

where b is the mini-batch size and ϵ is a small constant to prevent division by zero.

References

- [1] M. Arjovsky, A. Shah, and Y. Bengio. Unitary evolution recurrent neural networks. In *International Conference on Machine Learning*, pages 1120–1128, New York, USA, June 2016.
- [2] O. Can, K. Kapanova, and A. Søgaard. Gates create slow modes in recurrent neural networks. In *International Conference on Learning Representations (ICLR)*, 2020.
- [3] A. Cenì. Random orthogonal additive filters: A solution to the vanishing/exploding gradient of deep neural networks. *IEEE Transactions on Neural Networks and Learning Systems*, 36(6):10794–10807, 2025. doi: 10.1109/TNNLS.2025.3538924.
- [4] B. Chang, M. Chen, E. Haber, and E. H. Chi. AntisymmetricRNN: A dynamical system view on recurrent neural networks. In *International Conference on Learning Representations*, 2019. URL <https://openreview.net/forum?id=ryxepo0cFX>.
- [5] M. Chen, J. Pennington, and S. Schoenholz. Dynamical isometry and a mean field theory of RNNs: Gating enables signal propagation in recurrent neural networks. In J. Dy and A. Krause, editors, *Proceedings of the 35th International Conference on Machine Learning*, volume 80 of *Proceedings of Machine Learning Research*, pages 873–882, Stockholm, Sweden, 10–15 Jul 2018. PMLR.
- [6] K. Cho, B. Van Merriënboer, C. Gulcehre, D. Bahdanau, F. Bougares, H. Schwenk, and Y. Bengio. Learning phrase representations using RNN encoder-decoder for statistical machine translation. *arXiv preprint arXiv:1406.1078*, 2014.
- [7] N. B. Erichson, O. Azencot, A. Queiruga, L. Hodgkinson, and M. W. Mahoney. Lipschitz recurrent neural networks. *arXiv preprint arXiv:2006.12070*, 2021.
- [8] D. Gilboa, B. Chang, M. Chen, G. Yang, S. S. Schoenholz, E. H. Chi, and J. Pennington. Dynamical isometry and a mean field theory of lstms and grus. *arXiv preprint arXiv:1901.08987*, 2019.
- [9] A. Gu, K. Goel, and C. Ré. Efficiently modeling long sequences with structured state spaces. *arXiv preprint arXiv:2111.00396*, 2021.
- [10] A. Gu, I. Johnson, K. Goel, K. K. Saab, T. Dao, A. Rudra, and C. Ré. Combining recurrent, convolutional, and continuous-time models with linear state space layers. In *Thirty-Fifth Conference on Neural Information Processing Systems*, 2021.
- [11] K. Helfrich, D. Willmott, and Q. Ye. Orthogonal recurrent neural networks with scaled Cayley transform. In J. Dy and A. Krause, editors, *Proceedings of the 35th International Conference on Machine Learning*, volume 80 of *Proceedings of Machine Learning Research*, pages 1969–1978. PMLR, 10–15 Jul 2018.
- [12] N. J. Higham. *Functions of Matrices: Theory and Computation*. SIAM, 2008.
- [13] S. Hochreiter and J. Schmidhuber. Long short-term memory. *Neural Computation*, 9(8):1735–1780, 1997.
- [14] H. Jaeger, M. Lukoševičius, D. Popovici, and U. Siewert. Optimization and applications of echo state networks with leaky-integrator neurons. *Neural Networks*, 20(3):335–352, 2007. doi: 10.1016/j.neunet.2007.04.016.
- [15] A. Kag, Z. Zhang, and V. Saligrama. RNNs incrementally evolving on an equilibrium manifold: A panacea for vanishing and exploding gradients? In *International Conference on Learning Representations*, 2020.

[16] G. Kerg, K. Goyette, M. P. Touzel, G. Gidel, E. Vorontsov, Y. Bengio, and G. Lajoie. Non-normal recurrent neural network (nnrnn): learning long time dependencies while improving expressivity with transient dynamics. *arXiv preprint arXiv:1905.12080*, 2019.

[17] D. Kingma and J. Ba. Adam: A method for stochastic optimization. *arXiv preprint arXiv:1412.6980*, 2014.

[18] J. Koutnik, K. Greff, F. Gomez, and J. Schmidhuber. A clockwork RNN. In *International Conference on Machine Learning*, volume 32, pages 1863–1871, 2014.

[19] S. G. Krantz and H. R. Parks. *The Implicit Function Theorem: History, Theory, and Applications*. Birkhäuser, Boston, MA, 2003. doi: 10.1007/978-0-8176-8230-9.

[20] A. Krishnamurthy, C. Gehring, D. K. Misra, and C. Zhang. Theory of gating in recurrent neural networks. *Journal of Machine Learning Research*, 23(157):1–39, 2022.

[21] J. Lee, L. Xiao, S. Schoenholz, Y. Bahri, R. Novak, J. Sohl-Dickstein, and J. Pennington. Wide neural networks of any depth evolve as linear models under gradient descent. *Advances in neural information processing systems*, 32, 2019.

[22] Z. Mhammedi, A. Hellicar, A. Rahman, and J. Bailey. Efficient orthogonal parametrisation of recurrent neural networks using householder reflections. In *Proceedings of the 34th International Conference on Machine Learning*, page 2401–2409, 2017.

[23] N. Muca Cirone, A. Orvieto, B. Walker, C. Salvi, and T. Lyons. Theoretical foundations of deep selective state-space models. *Advances in Neural Information Processing Systems*, 37:127226–127272, 2024.

[24] R. Pascanu, T. Mikolov, and Y. Bengio. On the difficulty of training recurrent neural networks. In *Proceedings of the 30th International Conference on Machine Learning*, volume 28, pages 1310–1318, Atlanta, Georgia, USA, 2013.

[25] J. Pennington, S. Schoenholz, and S. Ganguli. Resurrecting the sigmoid in deep learning through dynamical isometry: theory and practice. In *Advances in Neural Information Processing Systems*, pages 4785–4795, 2017.

[26] R. Quax, D. Kandhai, and P. M. A. Sloot. Adaptive time scales in recurrent neural networks. *Scientific Reports*, 10(1):7442, 2020.

[27] S. Ruder. An overview of gradient descent optimization algorithms. *arXiv preprint arXiv:1609.04747*, 2016.

[28] T. K. Rusch and S. Mishra. Coupled oscillatory recurrent neural network (cornn): An accurate and (gradient) stable architecture for learning long time dependencies. *ICLR*, 2021.

[29] T. K. Rusch, S. Mishra, N. B. Erichson, and M. W. Mahoney. Long expressive memory for sequence modeling. *arXiv preprint arXiv:2110.04744*, 2021.

[30] A. M. Saxe, J. L. McClelland, and S. Ganguli. Exact solutions to the nonlinear dynamics of learning in deep linear neural networks. *arXiv preprint arXiv:1312.6120*, 2013.

[31] C. Tallec and Y. Ollivier. Can recurrent neural networks warp time? In *International Conference on Learning Representations*, 2018. URL <https://openreview.net/forum?id=SJcKhk-Ab>.

[32] M. O. Turkoglu, S. D’Aronco, J. D. Wegner, and K. Schindler. Gating revisited: Deep multi-layer rnns that can be trained. *IEEE Transactions on Pattern Analysis and Machine Intelligence*, 44(8):4081–4092, 2022. doi: 10.1109/TPAMI.2021.3064878.

- [33] J. Van Der Westhuizen and J. Lasenby. The unreasonable effectiveness of the forget gate. *arXiv preprint arXiv:1804.04849*, 2018.
- [34] A. Vaswani, N. Shazeer, N. Parmar, J. Uszkoreit, L. Kaiser, and I. Polosukhin. Attention is all you need. In *Advances in Neural Information Processing Systems*, 2017.
- [35] E. Vorontsov, C. Trabelsi, S. Kadoury, and C. Pal. On orthogonality and learning recurrent networks with long term dependencies. In *Proceedings of the 34th International Conference on Machine Learning*, page 3570–3578, 2017.
- [36] P. J. Werbos. Backpropagation through time: what it does and how to do it. *Proceedings of the IEEE*, 78(10):1550–1560, 1990.
- [37] S. Wisdom, T. Powers, J. Hershey, J. Le Roux, and L. Atlas. Full-capacity unitary recurrent neural networks. In D. D. Lee, M. Sugiyama, U. V. Luxburg, I. Guyon, and R. Garnett, editors, *Advances in Neural Information Processing Systems*, pages 4880–4888. Curran Associates, Inc., Barcelona, Spain, Dec. 2016.
- [38] N. Zucchetti and A. Orvieto. Recurrent neural networks: vanishing and exploding gradients are not the end of the story. *Advances in Neural Information Processing Systems*, 37:139402–139443, 2024.